Center for Turbulence Research
Proceedings of the Summer Program 1992

Numerical simulations of turbulent premixed $H_2/O_2/N_2$ flames with complex chemistry

By M. Baum,[1] T. J. Poinsot,[2] AND D. C. Haworth[3]

Premixed stoichiometric $H_2/O_2/N_2$ flames propagating in two–dimensional turbulence have been studied using direct numerical simulation (simulations in which all fluid and thermochemical scales are fully resolved) including realistic chemical kinetics and molecular transport. Results are compared with earlier zero–chemistry (flame sheet) and one–step chemistry simulations. Consistent with the simpler models, the turbulent flame with realistic chemistry aligns preferentially with extensive strain rates in the tangent plane and flame curvature probability density functions are close to symmetric with near–zero means. By contrast to simple–chemistry results with non–unity Lewis numbers (ratio of thermal to species diffusivity), local flame structure does not correlate with curvature but rather with tangential strain rate. Turbulent straining results in substantial thinning of the flame relative to the steady unstrained laminar case. Heat release and H_2O_2 contours remain thin and connected ('flamelet–like') while species including H–atom and OH are more diffuse. Peak OH concentration occurs well behind the peak heat–release zone. This work suggests the feasibility of incorporating realistic chemistry into full turbulence simulations to address issues such as pollutant formation in hydrocarbon–air flames.

1. Introduction

Turbulent premixed combustion in practical devices is a complex phenomenon combining chemical kinetics, molecular transport, and hydrodynamic turbulence in difficult geometric configurations. Increasing regulative and competitive pressures demand improved physical understanding and predictive modeling capability for combustion phenomena including ignition, quenching, and pollutant formation. For example, many governments impose limits on emissions of oxides of nitrogen, carbon monoxide, and unburned hydrocarbons from gasoline–fueled spark–ignited automotive engines. Pending regulations in the United States seek further reductions in the allowable levels of these pollutants and provide for species differentiation in hydrocarbon emissions to account for the relative propensity of different components to promote ozone formation in the atmosphere. Many aspects of chemical kinetics (e.g. aromatic hydrocarbon chemistry, Westbrook 1991) are poorly understood even at a fundamental level and emissions models for engineering applications remain largely

1 Ecole Centrale, Paris
2 C.N.R.S., Institut de Mecanique des Fluides de Toulouse, France
3 General Motors Research & Environmental Staff, Warren, MI

empirical. Thus complex chemical kinetics in turbulent premixed combustion is a crucial topic for research and modeling.

Both experimental and numerical investigations of chemical kinetics influences in turbulent premixed combustion are complicated by the strong coupling of hydrodynamics with thermochemistry and by resolution requirements: hydrodynamic and thermochemical spatial and temporal scales span many orders of magnitude in premixed flames at high Reynolds and Damköhler numbers (the latter being the ratio of a characteristic flow time scale to chemical time scales). Thus direct numerical simulation (DNS) of practical turbulent premixed flames is impracticable at present and will remain so for the foreseeable future. (Here and in the following, 'DNS' is taken to mean simulations in which all scales of motion are fully resolved both spatially and temporally so that no turbulence modeling – explicit spatial or temporal filtering – is employed.) Idealized model problems are amenable to numerical analysis, and carefully designed numerical simulations are well suited to isolating specific phenomena and extracting fundamental physical understanding. However, one must remain wary in extrapolating results from idealized model problems to practical combustion systems.

Numerical combustion studies have tended to proceed along one of two parallel paths. Either detailed chemical kinetics models have been implemented in simple flow configurations (one–dimensional laminar, e.g. Warnatz 1981, Drake & Blint 1988; axisymmetric laminar, e.g. Smooke *et al.* 1990), or turbulence simulations have been performed with embedded simple–chemistry models (zero–chemistry or flame sheet, e.g. Kerstein *et al.* 1988, Girimaji & Pope 1992; zero–heat–release one–step Arrhenius, e.g. Rutland *et al.* 1990; one–step Arrhenius with heat release, e.g. Haworth & Poinsot 1992). The detailed chemistry scheme for methane–air oxidation employed by Xu & Smooke (1991) includes 26 species and 45 reactions. Solving the resulting stiff system of convection/diffusion/reaction equations for a *laminar* axisymmetric Bunsen burner flame requires on the order of 100 CPU hours using state–of–the–art numerical algorithms on a high–end workstation ($\sim$ 26 Mflops). This is the same order of computational resources as that required for DNS of *nonreacting* homogeneous isotropic turbulence at a Taylor–scale Reynolds number of $Re_\lambda \approx 90$ (Pope 1991).

The present research represents an attempt to bridge the two numerical approaches by coupling complex chemistry and full turbulence simulations. Here H_2–O_2 chemistry (inert N_2 diluent) has been modeled using a nine–species, 19–reactant scheme (Miller *et al.* 1982) including detailed molecular transport in two–dimensional isotropic turbulence. Specific goals are threefold. First, we wish to explore the feasibility of complex–chemistry DNS for future application to more complex thermochemical systems (e.g. hydrocarbon fuels). Ignition, quenching, and pollutant formation issues are of practical interest in such systems. Second, we will compare results obtained using the present detailed–chemistry scheme to those obtained earlier using simpler zero– and one–step chemistry models. In particular we are interested in statistics of strain rate, curvature, and local burning rate along the flame front and the robustness of flamelet models with realistic kinetics. Finally,

we will compare the local structure of the turbulent premixed flame with detailed kinetics to that of an unstrained laminar flame having the same thermochemical properties. Questions of interest include possible shifts in radicals relative to laminar profiles and which radical species might best be suited to marking the region of peak heat release in experiments.

2. Background: DNS of turbulent premixed combustion

DNS has proved to be a valuable tool in addressing fundamental physical questions and in the construction of models for turbulent premixed combustion. The past several years have seen DNS applied to a hierarchy of premixed systems of increasing complexity. Results of these simulations generally have been interpreted in the framework of the flamelet regime of combustion wherein a thin laminar-like reaction zone separates unburnt gas from hot burnt products. (In propagating-interface type models, this structure is imposed.) Roughly speaking, flamelet combustion corresponds to conditions where the largest chemical scales are small compared with the smallest hydrodynamic scales: however, it has proven to be a worthwhile framework in which to interpret results even in cases where turbulence microscales are smaller than the flame thickness (Haworth & Poinsot 1992). Moreover, flamelet models are widely used as combustion 'submodels' in Reynolds-averaged computations of premixed turbulent combustion in engineering applications (e.g. El Tahry 1990, Boudier *et al.* 1992).

2.1. Propagating-interface (zero-chemistry) models

Analytic studies of the kinematics of a propagating surface in turbulent flow have resulted in relationships that provide a basis for flamelet models and for interpreting numerical simulation results. For example, the roles of hydrodynamic straining and flame curvature in modifying the area A of a propagating surface element are expressed in the relationship (Pope 1988, Candel & Poinsot 1990),

$$\frac{1}{A}\frac{dA}{dt} = a_t + \frac{s_d}{\mathcal{R}} \,. \tag{1}$$

Here a_t is the hydrodynamic strain rate in the plane tangent to the surface, s_d is the speed of advance of the propagating surface relative to the fresh gas, and $\mathcal{R}$ is the radius of curvature ($\mathcal{R} < 0$ for surface elements propagating towards the center of curvature, e.g. concave towards reactants for the premixed flame). This relationship motivates attempts to isolate strain-rate from curvature effects in turbulent premixed combustion, even though the two are not completely independent (Pope 1988, Haworth & Poinsot 1992).

Numerical simulations (DNS) incorporating propagating surface models have proceeded via a variety of front-tracking algorithms (reviewed in Oran & Boris 1987), field-equation approaches (Kerstein *et al.* 1988, Ashurst *et al.* 1988), and statistical ensembles of infinitesimal surface elements (Girimaji & Pope 1992). These zero-chemistry flame-sheet models have contributed significantly to our understanding of flame topology and have provided quantitative information on statistical correlations that is useful in the construction and calibration of models of turbulent

premixed combustion in the flamelet regime (e.g. Bray & Cant 1991). The influence of chemical kinetics effects in such models generally is felt only through the propagation speed, whose dependence on thermochemical and/or turbulence parameters must be prescribed.

2.2. *Simple-chemistry models*

Studies of the dynamic interactions between fluid flow and finite-rate chemistry in flamelet or non-flamelet regimes require that the flame structure be resolved. However, the addition of chemical length and time scales that are of the order of or smaller than the smallest turbulence scales implies that, for a given spatial and temporal resolution, a smaller range of hydrodynamic scales can be simulated compared to computations in which the flame has no internal structure. Two-dimensional vortex methods have been used to study interactions between turbulent fluid flow and finite-rate chemistry by a number of authors including Ashurst & Barr (1983), Ghoniem & Krishnan (1988), and Ashurst *et al.* (1987). Three-dimensional simulations including finite-rate chemistry (constant density, zero heat release, single-step Arrhenius chemistry) have been reported by Rutland *et al.* (1990): results included distributions of local burning rate over a range of Damköhler numbers. Further three-dimensional constant-density simulations been published by El Tahry *et al.* (1991) Rutland & Trouvé (1990) (a study of Lewis number effects) and by Cant *et al.* (1990) (a study of statistics relevant to the Bray-Moss-Libby model of turbulent premixed combustion).

The present work follows a number of two-dimensional simulations with variable fluid properties and heat release (Poinsot 1991; Poinsot *et al.* 1990, 1991, 1992; Meneveau & Poinsot 1990, Haworth & Poinsot 1992, Poinsot & Haworth 1992). Contributions of these studies include a characterization of the scales of turbulent motion that influence flame structure (Poinsot *et al.* 1990, 1991), investigations of flame quenching (Poinsot *et al.* 1991, Meneveau & Poinsot 1990), identification of Lewis number effects (Haworth & Poinsot 1992), a study of ignition and early flame-kernel growth (Poinsot 1991), and a model for flame-wall interactions (Poinsot & Haworth 1992). Compared to three-dimensional constant-property simulations, two-dimensional variable-density simulations allow a wider dynamic range of scales and full two-way fluid-chemistry coupling. Values of relevant dimensionless parameters in the present study are given in Section 3.

However, the dynamics of two-dimensional turbulence are not identical to those of three-dimensional turbulence (Batchelor 1953, Herring *et al.* 1974, Lesieur 1987). In particular, the vortex-stretching mechanism for the cascade of energy to progressively smaller scales of motion is absent in two dimensions and the smallest scales of motion do not follow the usual Kolmogorov scaling. Thus the statistics of small-scale quantities especially are expected to differ between two-dimensional and three-dimensional simulations. Partial justification for the appropriateness of two-dimensional studies of premixed flame structure can be found in three-dimensional results: the topology of a propagating surface in three-dimensional turbulence has been found to be primarily two-dimensional, particularly those surface elements having the highest curvatures (Ashurst 1990, Cant *et al.* 1990, Girimaji & Pope

1992). That is, a flame tends to be locally cylindrical rather than spherical in shape. Further *a posteriori* justification can be found in the two–dimensional results themselves, where many features in common with the three–dimensional findings have been noted (Haworth & Poinsot 1992). Common results include: preferential alignment of the flame with extensive strain rates in the tangent plane; scaling of flame–area–averaged mean tangential strain rate with turbulence micro–timescales; and nearly symmetric pdf's of flame curvature having near–zero mean.

The present work follows most immediately the study of nonunity Lewis number effects (Le = ratio of thermal to species diffusivity) in two–dimensional turbulent premixed combustion reported by Haworth & Poinsot (1992). In addition to the results already discussed, it was found that for $Le = 1$, the local burning velocity of the turbulent flame is everywhere nearly identical to that of an undisturbed laminar flame; for nonunity Lewis numbers, the local burning velocity differs from that of the laminar flame and correlates strongly with the local flame curvature; curvature effects cancel out in the mean to leave the mean extensive tangential strain rate as the principal influence on the mean burning velocity of the turbulent flame; and thermodiffusive effects result in more flame area for $Le < 1$ than for $Le > 1$. It was further argued that these molecular transport effects should remain important at higher Reynolds numbers and for complex chemistry, provided that a single global deficient–reactant–based Lewis number can be defined. Here the simulations are extended from one–step chemistry with simple transport to realistic chemistry and transport, permitting a direct assessment of the second claim. We continue to adopt a flamelet viewpoint for diagnostics and analysis.

3. Problem definition

3.1. Governing equations and numerical methods

The set of equations solved is the compressible multi–species reacting flow equations comprising conservation of mass, linear momentum, energy, and N_s species mass fractions. In Cartesian tensor notation (no sum on Greek indices),

$$\frac{\partial \rho}{\partial t} + \frac{\partial \rho u_j}{\partial x_j} = 0 \,, \tag{2}$$

$$\frac{\partial \rho u_i}{\partial t} + \frac{\partial \rho u_i u_j}{\partial x_j} = -\frac{\partial p}{\partial x_i} + \frac{\partial \tau_{ij}}{\partial x_j} \,, \tag{3}$$

$$\frac{\partial \rho e_t}{\partial t} + \frac{\partial (\rho e_t + p) u_j}{\partial x_j} = \frac{\partial (u_j \tau_{ij})}{\partial x_i} - \frac{\partial q_j}{\partial x_j} \,, \tag{4}$$

$$\frac{\partial \rho Y_\alpha}{\partial t} + \frac{\partial \rho Y_\alpha u_j}{\partial x_j} = -\frac{\partial \rho Y_\alpha V_{\alpha j}}{\partial x_j} + W_\alpha \dot{\omega}_\alpha \,. \tag{5}$$

Here u_i is the i^{th} component of the fluid velocity, e_t is the total energy density per unit mass, and Y_α, $\alpha = 1, \ldots, N_s$, is the mass fraction of species α. The fluid mass density is ρ, p is the thermodynamic pressure, and τ_{ij} and q_j are, respectively, the

viscous stress tensor and the heat flux vector. The molar chemical production rate of species α is $\dot{\omega}_\alpha$ while W_α is its molecular weight. The variable $V_{\alpha j}$ is the diffusion velocity for species α.

The set of governing equations is closed with the ideal gas equation of state and constitutive relations,

$$p = \rho RT \,, \tag{6}$$

$$\tau_{ij} = \overline{\mu}\left(\frac{\partial u_i}{\partial x_j} + \frac{\partial u_j}{\partial x_i} - \frac{2}{3}\delta_{ij}\frac{\partial u_k}{\partial x_k}\right) \,, \tag{7}$$

$$e_t = \frac{1}{2}u_k u_k + e \,, \tag{8}$$

$$e = \sum_{\alpha=1}^{N_s} h_\alpha Y_\alpha - \frac{p}{\rho} \,, \tag{9}$$

$$h_\alpha(T_1) = \Delta h^0_{f\alpha} + \int_{T_0}^{T_1} C_{p\alpha}(T)dT \,, \tag{10}$$

$$q_j = -\overline{\lambda}\frac{\partial T}{\partial x_j} + \rho\sum_{\alpha=1}^{N_s} h_\alpha Y_\alpha V_{\alpha j} \,. \tag{11}$$

In these equations, $\overline{\mu}$ and $\overline{\lambda}$ are, respectively, the mean viscosity and thermal conductivity. The formation enthalpy of species α at the reference temperature T_0 is $\Delta h^0_{f\alpha}$, and h_α is the enthalpy of species α. (Here the reference state is T_0 =298.15 K.)

Species molecular transport is modeled using Fick's law. An effective species diffusivity D_α is computed as follows:

$$D_\alpha = \frac{(1 - Y_\alpha)}{\sum\limits_{\beta=1,\beta\neq\alpha}^{N_s} X_\beta / D_{\alpha\beta}} \,, \tag{12}$$

where $D_{\alpha\beta}$ are the binary diffusion coefficients and X_α is the mole fraction of species α. Diffusion coefficients are related to the diffusion velocity $\mathcal{V}_{\alpha j}$ by,

$$\mathcal{V}_{\alpha j} = -\frac{D_\alpha}{X_\alpha}X_{\alpha,j} \,. \tag{13}$$

The diffusion velocities resulting from Eqs. (12) and (13) do not, in general, satisfy conservation of mass. A correction velocity V_{cj} is added such that the net diffusive flux is equal to zero,

$$\sum_{\alpha=1}^{N_s} Y_\alpha V_\alpha j = 0 \,. \tag{14}$$

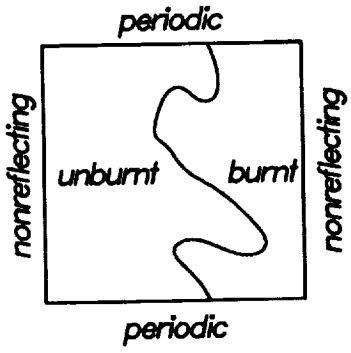

FIGURE 1. Schematic of computational domain: a premixed flame separates unburnt reactants from burnt products.

Finally, we have,

$$V_{\alpha j} = \mathcal{V}_{\alpha j} + V_{cj} = -\frac{D_\alpha}{X_\alpha} X_{\alpha,j} + \frac{\sum_{\beta=1}^{N_s} Y_\beta (D_\beta / X_\beta) X_{\beta,j}}{\sum_{\beta=1}^{N_s} Y_\beta} . \tag{15}$$

Species production rates are given by the Arrhenius law with (forward) rate constants $k_{f\alpha}$ of the form,

$$k_{f\alpha} = A_\alpha T^{\beta_\alpha} exp(-E_{0\alpha}/R_0 T) , \tag{16}$$

where R_0 is the universal gas constant. Hydrogen–oxygen kinetics has been modeled using the nine–species, 19–reaction scheme devised by Miller *et al.* (1982). Coefficients for this scheme are summarized in Table I. Fluid properties, molecular transport coefficients, and reaction source terms are computed using CHEMKIN and TRANSPORT (Kee *et al.* 1980, Kee *et al.* 1983).

Using these assumptions and a Cartesian frame of reference, the conservation equations are solved using a high–order finite–difference scheme (Lele 1992). The calculations are initialized with reactants on one side of the computational domain and products on the other; these are separated by a laminar premixed flame (Figure 1). The initial laminar profiles are themselves steady one–dimensional solutions to Eqs. (2)–(16). On lateral boundaries, periodic conditions are enforced while non–reflecting boundary conditions are used on inflow/outflow boundaries (Poinsot & Lele 1992). Isotropic two–dimensional turbulence is prescribed with a turbulence spectrum that is the same as that used in earlier studies (e.g. Haworth & Poinsot 1992). Two parameters suffice to define the initial energy spectrum: the rms turbulence velocity $u_p = u'(t = 0)$ and the peak energy wavelength L_i. These and other relevant parameters are summarized in Table II.

Table I. Reaction mechanism rate coefficients in the form $k_f = AT^{\beta}exp(-E_0/R_0T)$ (Eq. 16) (Miller *et al.* 1982). Units are moles, cubic centimeters, seconds, degrees K, and calories/mole. Species: H_2 O_2 OH O H H_2O HO_2 H_2O_2 N_2.

#	Reaction	A	β	E_0
R_1	$H_2 + O_2 \rightleftharpoons 2\ OH$	1.7×10^{13}	0.	47780
R_2	$H_2 + OH \rightleftharpoons H_2O + H$	1.17×10^{9}	1.3	3626
R_3	$H + O_2 \rightleftharpoons OH + O$	5.13×10^{16}	−0.816	16507
R_4	$O + H_2 \rightleftharpoons OH + H$	1.8×10^{10}	1.0	8826
R_5	$H + O_2 + M \rightleftharpoons HO_2 + M^a$	2.1×10^{18}	−1.0	0
R_6	$H + 2\ O_2 \rightleftharpoons HO_2 + O_2$	6.7×10^{19}	−1.42	0
R_7	$H + O_2 + N_2 \rightleftharpoons HO_2 + N_2$	6.7×10^{19}	−1.42	0
R_8	$OH + HO_2 \rightleftharpoons H_2O + O_2$	5×10^{13}	0.	1000
R_9	$H + HO_2 \rightleftharpoons 2\ OH$	2.5×10^{14}	0.	1900
R_{10}	$O + HO_2 \rightleftharpoons O_2 + OH$	4.8×10^{13}	0.	1000
R_{11}	$2\ OH \rightleftharpoons O + H_2O$	6×10^{8}	1.3	0
R_{12}	$H_2 + M \rightleftharpoons H + H + M^b$	2.23×10^{12}	0.5	92600
R_{13}	$O_2 + M \rightleftharpoons O + O + M$	1.85×10^{11}	0.5	95560
R_{14}	$H + OH + M \rightleftharpoons H_2O + M^c$	7.5×10^{23}	−2.6	0
R_{15}	$HO_2 + H \rightleftharpoons H_2 + O_2$	2.5×10^{13}	0.	700
R_{16}	$2\ HO_2 \rightleftharpoons H_2O_2 + O_2$	2×10^{12}	0.	0
R_{17}	$H_2O_2 + M \rightleftharpoons OH + OH + M$	1.3×10^{17}	0.	45500
R_{18}	$H_2O_2 + H \rightleftharpoons H_2 + HO_2$	1.6×10^{12}	0.	3800
R_{19}	$H_2O_2 + OH \rightleftharpoons H_2O + HO_2$	1.0×10^{13}	0.	1800

[a] Third-body efficiencies: $k(H_2) = 3.3k(Ar)$, $k(H_2O) = 21.0k(Ar)$.
[b] Third-body efficiencies: $k(H_2) = 3.0k(Ar)$, $k(H) = 2.0k(Ar)$, $k(H_2O) = 6.0k(Ar)$.
[c] Third-body efficiencies: $k(H_2O) = 20.0k(Ar)$.

In Table II, a subscript 'u' refers to properties in the unburnt reactants. Key parameters are: the rms turbulence intensity u', the turbulence integral length scale l based on two-point velocity correlations and timescale $\tau = l/u'$, and flame or chemical scales s_l^0 (the unstrained laminar flame speed), $\delta_l \equiv (T_b - T_u)/(dT/dx|_{max})$ (the laminar flame thickness), and $\tau_f = \delta_l/s_l^0$. The fuel mass equivalence ratio is Φ. There are $n_x \times n_y$ computational grid points in the $L_{box} \times L_{box}$ square computational domain.

The turbulence Reynolds numbers and ratio of rms turbulence intensity to laminar flame speed of Table II imply a regime of combustion where turbulence is intense compared to the laminar flame speed, and flames are thinner than the turbulence integral scale but are thicker than turbulence microscales. Turbulence and flame timescales are of the same order.

Table II. Initial parameters for two–dimensional simulations.

Case	Φ	T_u	p	s_l^0	δ_l	$Re_{L_i} = \frac{u_p L_i}{\nu}$	$Re_l = \frac{u' l}{\nu}$	u'/s_l^0	L_i/δ_l	l/δ_l	τ/τ_f	L_{box}	$n_x = n_y$
	[–]	[K]	[kPa]	[m/s]	[cm]	[–]	[–]	[–]	[–]	[–]	[–]	[cm]	[–]
1	1.0	800	101	19.5	0.044	2000	650	2.1	6.3	2.0	0.48	2.00	487
2	1.0	800	101	19.5	0.044	4000	1300	4.2	12.7	4.0	0.95	1.24	301

3.2. Diagnostics

Postprocessing of the two–dimensional computed fields (snapshots at fixed times) begins by defining a flame front as an isocontour of reactant mass fraction or temperature. Here we have used $Y_{O_2} = 0.22$, corresponding to the position of peak heat release in the laminar flame (Figure 2). Once the flame front has been located, the local normal and local curvature are readily computed. Curvatures concave towards the hot products are taken to be positive. One–dimensional cuts normal to the flame are taken: it is these profiles that define the local 'structure' of the turbulent flame. We compare the local turbulent flame profiles with the steady unstrained one–dimensional laminar flame profile for the same chemistry and fluid properties. Of particular interest is the distribution along the flame of the normalized local flame speed ('flamelet speed') s_n defined as the integral of the heat–release profile in a direction locally normal to the flame. The local heat–release rate $\dot{w}_Q$ is defined by,

$$\dot{w}_Q = \sum_{\alpha=1}^{N_s} \dot{w}_\alpha \Delta h_{f\alpha}^0 \,, \tag{17}$$

and the normalized flamelet speed is then,

$$s_n = \int \dot{w}_Q \, dn \, / \, s_{n0} \,. \tag{18}$$

A normalized flame length $\mathcal{L}^*$ and turbulent flame speed s_T^* are defined as,

$$\mathcal{L}^* \equiv L_{flame}/L_{flame\,0} \,, \tag{19}$$

$$s_T^* \equiv \overline{\dot{w}_Q} \, / \, \overline{\dot{w}_{Q0}} \; = \; \langle s_n \rangle \mathcal{L}^* \,. \tag{20}$$

In Eqs. (18)–(20), the subscript '0' denotes the value for the unstrained planar laminar flame; overbars denote volume (area) averages while angled brackets are reserved for flame–area–weighted means (length–weighted in two spatial dimensions). A check of self–consistency is to verify the equality between s_T^* calculated in the two ways given in Eq. (20): they are found to agree to within a few percent in all cases.

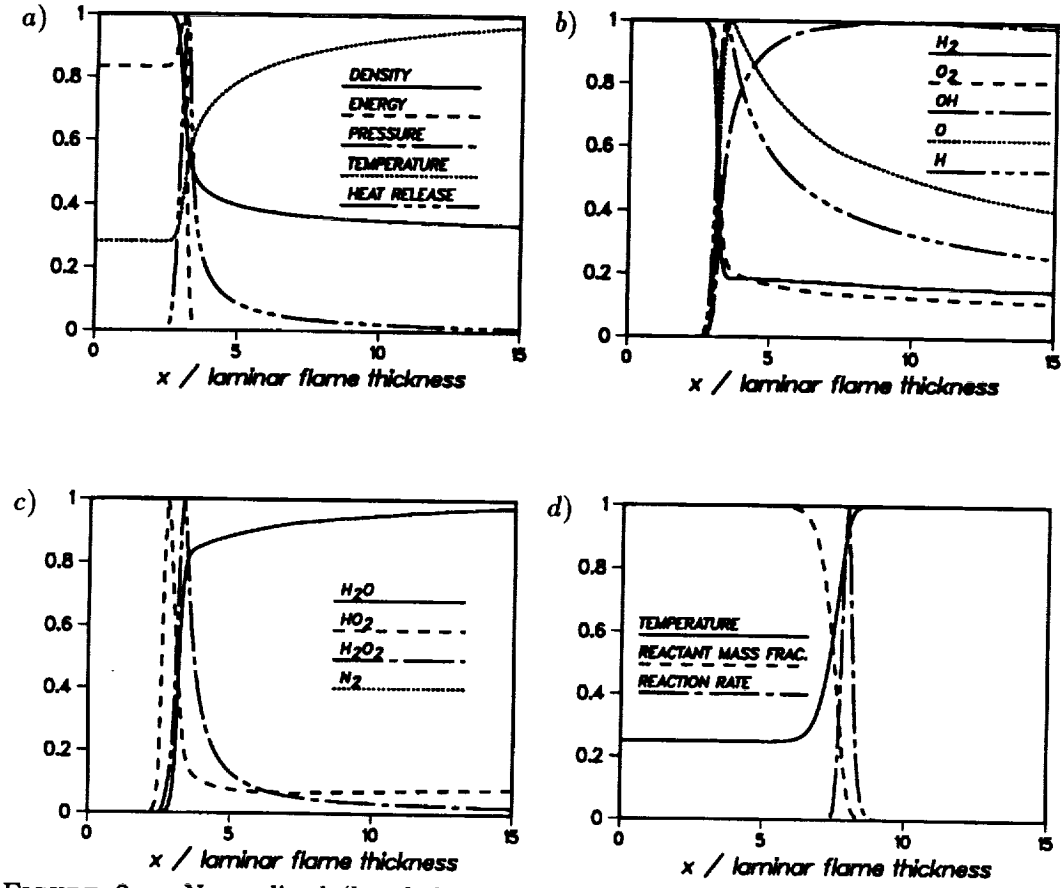

FIGURE 2. Normalized (by their maxiumum value) steady unstrained laminar flame profiles: a)–c) complex chemistry (Tables I and II); d) one–step chemistry $\dot{w} = \Lambda\rho Y \exp\left(\frac{-\beta(1-\Theta)}{1-\alpha(1-\Theta)}\right)$, $\Theta = (T - T_u)/(T_b - T_u)$, $\alpha = 0.75$, $\beta = 8.0$, $\Lambda = 146$ (Haworth & Poinsot 1992).

4. Results

4.1. Laminar profiles

Profiles of the steady one–dimensional laminar solution are displayed in Figure 2a–c, where each quantity has been normalized by its maximum value. Corresponding profiles for the one–step Arrhenius scheme used in Haworth & Poinsot (1992) are shown in Figure 2d. The abscissa is in units of the laminar flame thickness δ_l, which is of the order of the heat–release zone thickness. A striking difference between the simple– and complex–chemistry temperature and species profiles is the extended tails into the burnt gas for the complex chemistry case. One might anticipate difficulty in maintaining this structure in turbulent flames: even in cases where all turbulence scales are larger than δ_l, turbulence may still be able to modify the laminar flame structure on the burnt side. Other noteworthy features of these profiles include the significant 'leakage' of fuel and oxidizer into the products, high

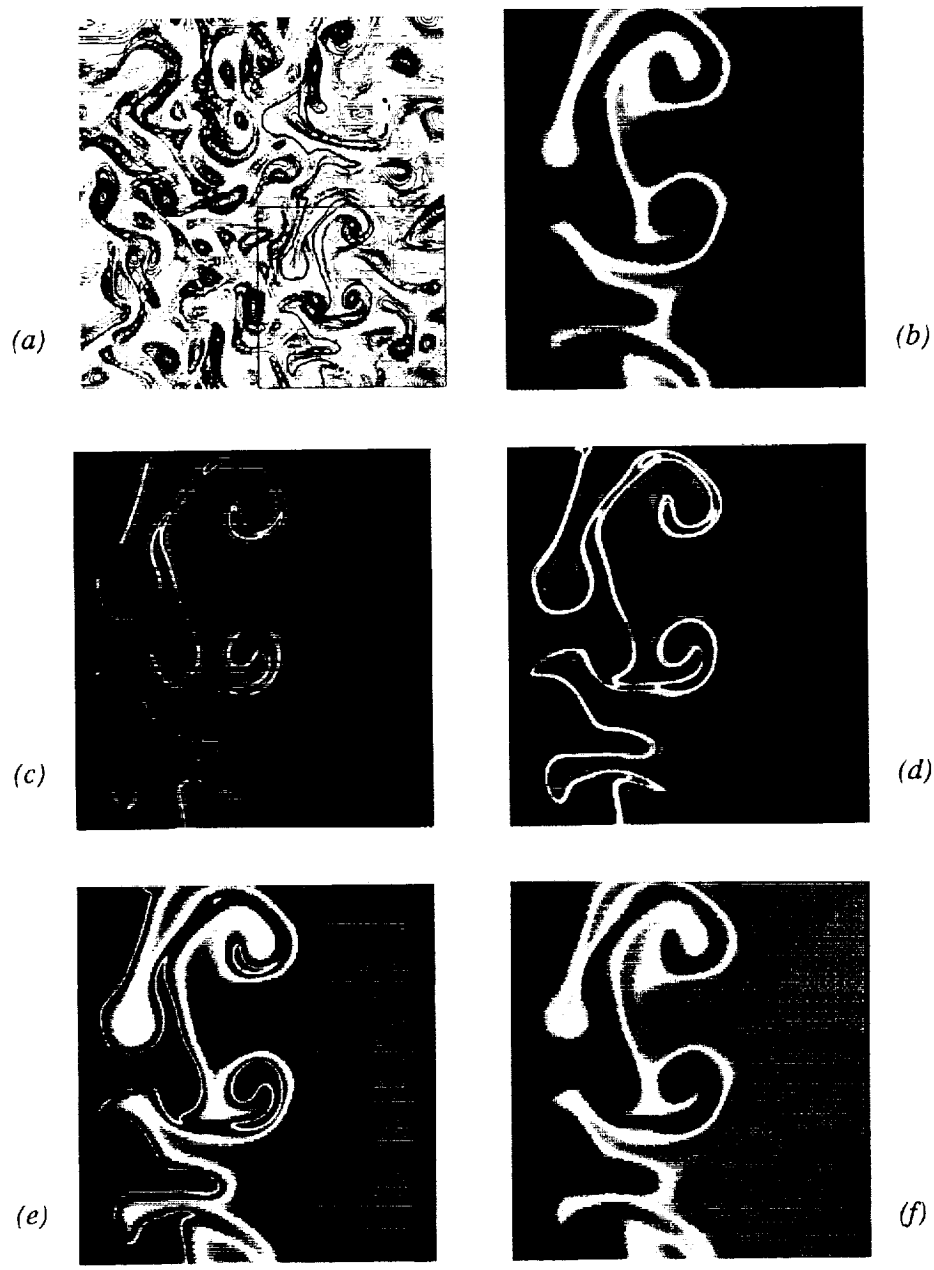

FIGURE 3. Computed fields at one instant of time, Case 1, time $t/\tau_f = 1.24$: a) vorticity contours with flame isocontour in magenta; b) temperature; c) heat release; d) H_2O_2 mass fraction; e) H mass fraction; f) OH mass fraction. Contour color scale ranges from blue (min) to red (max). In a), the full computational box is shown while b)-f) depict only the subdomain indicated by the black outline in a).

OH concentrations in the burnt gas, and locations of peak radical concentrations relative to peak heat release. The high product temperature (2840 K) is responsible for the high equilibrium H_2, O_2, and OH concentrations on the burnt side. Peak OH concentration occurs well behind the peak heat–release zone, while H– and O–atom, H_2 O_2, and HO_2 peak closer to the location of peak heat release.

4.2. Turbulent flame contours

Examples of computed fields at one instant of time for Case 1 at $t/\tau_f = 1.24$ are given in Figure 3 (unburnt gases are on the left, burnt products are on the right). The initially planar flame has been severely distorted by the turbulence by this time, even to the extent of tearing off pockets of fresh gas which are carried into the product side. Eventually these pockets of fresh gas are consumed for these adiabatic flames. Nevertheless, the structure of the underlying laminar flame remains readily recognizable. Heat release contours (Fig 3c) suggest a thin flamelet–like structure albeit with some islands of fresh gas burning enveloped by the hot products. Some radicals including H_2O_2 (Figure 3d) show similar behavior to the heat release: profiles remain thin and appear to mark the region of maximum heat release. On the other hand, H–atom levels (Figure 3e), while peaking close to the maximum heat–release zone, show a long diffuse tail on the burnt side, presumably a consequence of the high H diffusivity. Gradients in OH mass fraction are steep through the region of maximum heat release (Figure 3f) but peak OH occurs well behind the flame front and isocontours of high OH concentration do not remain connected on the burnt side. Most of these features might be anticipated from Figure 2a–c. Thus in the present case, OH does not serve as a good marker of the region of maximum heat release in the flame.

An example of the influence of turbulence parameters on flame structure is given in Figure 4. There the isocontour used to define the flame at one instant of time is plotted for Cases 1 and 2 at equal flame times $t/\tau_f = 0.36$ and at equal turbulence times $t/\tau_0 \approx 0.8$ ($\tau_0 = \tau(t = 0)$). The smaller integral scale of Case 1 yields a more highly wrinkled flame that, as illustrated in Figure 3, even shows pockets in the burnt gas at later times. Case 2, by contrast, yields a flame with large–scale folding versus fine–scale wrinkling.

4.3. Statistics of flame curvature, strain rate, and flamelet speed

Statistics of tangential strain rate, flame curvature, and local flamelet speed are presented in Figs. 5–9. Probability density functions (pdf's) of flame tangential strain rate and flame curvature are given in Figs. 5 and 6, respectively. Figure 5 confirms the findings of several earlier studies using zero– and single–step chemistry models: the turbulent flame aligns preferentially with extensive strain rates in the tangent plane (Ashurst 1990, Girimaji & Pope 1992, El Tahry *et al.* 1991, Cant *et al.* 1990, Rutland *et al.* 1990). Figure 6 also is reminiscent of results found using simpler models (Haworth & Poinsot 1992) and experiments (Lee *et al.* 1991): curvature pdf's are close to symmetric with near–zero mean curvature. While some skewing of the pdf's towards negative curvatures might be expected at low u'/s_l^0 (Rutland & Trouvé 1990, Becker *et al.* 1990), no such skewing is evident here. The

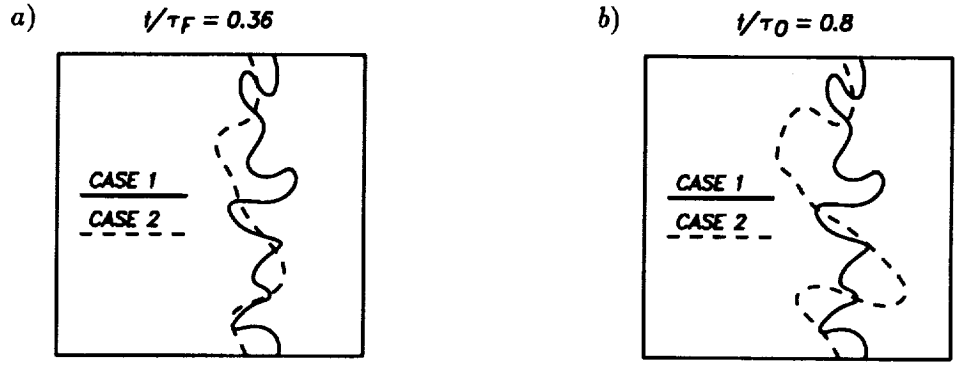

FIGURE 4. Isocontours $Y_{O_2} = 0.22$ for Cases 1 and 2 in a 1.24 cm × 1.24 cm region: a) $t/\tau_f = 0.36$; b) $t/\tau_0 \approx 0.8$.

more highly wrinkled nature of the Case 1 flame is manifested in the broader tails (higher rms) of the curvature pdf for Case 1 versus Case 2.

Scatter plots of local flamelet speed s_n versus local tangential strain rate and local flame curvature are given in Figs. 7 and 8, respectively. Each point in these two figures corresponds to a point sampled uniformly along the isocontour defining the turbulent flame. While no correlation of local burning velocity with curvature is evident, the decrease in s_n with increasing tangential strain rate is surprisingly strong. In fact, this correlation develops over time in the computations: at time $t = 0$, the normalized flamelet speed s_n is everywhere equal to unity. The flame-area-averaged normalized mean flamelet speed $\langle s_n \rangle$ decreases with time (Figure 9). Figure 9b, for example, portrays the evolution from the initial delta function pdf of flamelet speed at time $t = 0$ for Case 2: both the mean value $\langle s_n \rangle$ and the value of s_n at which the pdf peaks decrease with time as the flame develops (Table III).

No statistically steady state is achieved in the duration of the present computations. While the mean consumption rate per unit area of flame $\langle s_n \rangle$ (Eq. 18) is significantly smaller than unity, the increase in flame area $\mathcal{L}^*$ (Eq. 19) more than compensates to yield normalized turbulent flame speeds s_T^* (Eq. 20) that are greater than unity, as expected. The evolution of these global quantities with time is summarized in Table III.

Peak heat-release rates (not shown) remain within ±5% of the laminar value in all cases, suggesting that this reduction of local consumption rate $\langle s_n \rangle$ is primarily a flame thickness effect. These results are unexpected in view of the findings in Haworth & Poinsot (1992) for simple chemistry. There it was found that, for nonunity Lewis numbers, curvature dominated the local flame structure, and a correlation between local burning velocity and local tangential strain rate was evident only for $Le = 1$. In no case was the straining sufficiently high to yield the extremely low values of $\langle s_n \rangle$ found here. While the fuel-based (H_2) Lewis number in the present case is clearly less than unity, no single global deficient-reactant-based Lewis number can be unambiguously defined for $\Phi = 1$ (Chelliah & Williams 1987). Arguments by

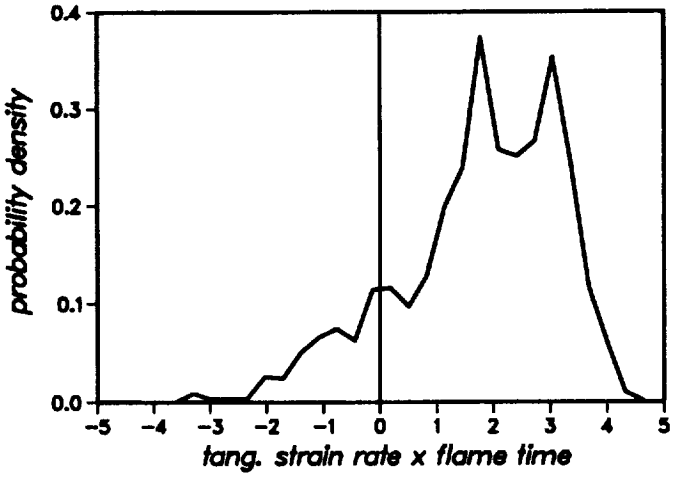

FIGURE 5. Pdf of normalized tangential strain rate, Case 1, $t/\tau_f = 0.36$: mean=1.816, rms=1.394.

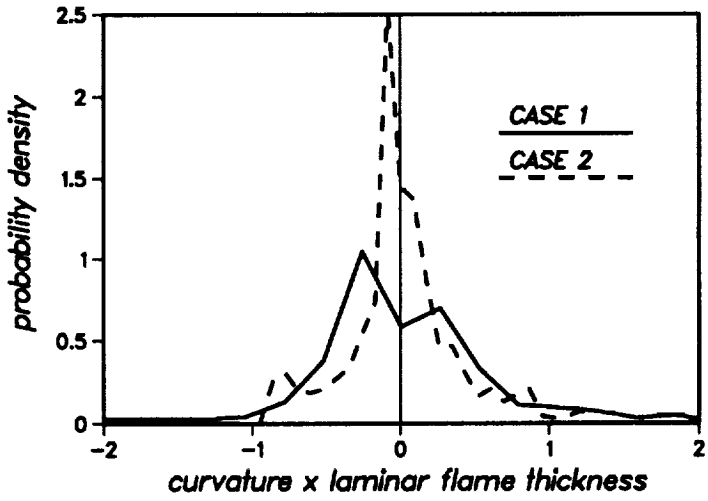

FIGURE 6. Pdf's of normalized flame curvature, $t/\tau_0 \approx 0.8$. Case 1: mean=0.0056, rms=0.82; Case 2: mean=0.0043, rms=0.35.

Joulin & Mitani (1981) suggest an equivalent Lewis number of somewhat less than unity for the present thermochemistry: however, the decreasing flamelet speed with increasing tangential strain rate of Figure 7 suggests that, if anything, the effective Lewis number may be greater than or equal to unity here.

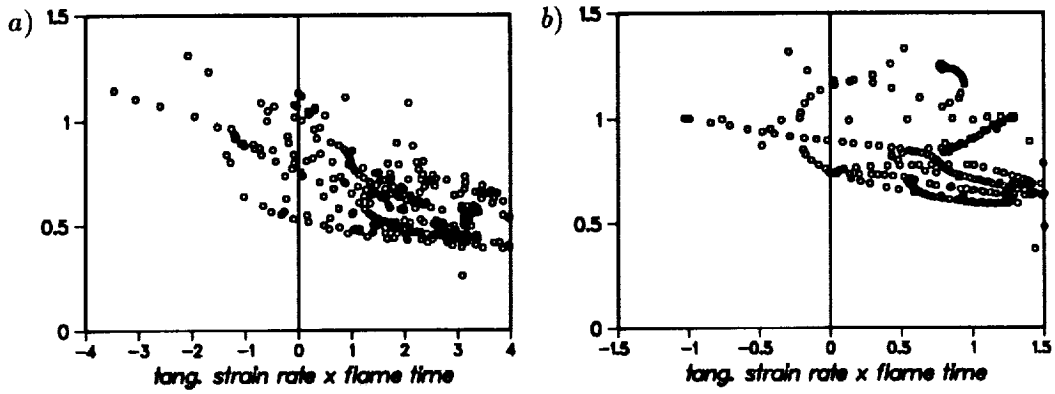

FIGURE 7. Scatter plots of normalized flamelet speed s_n (Eq. 18) versus normalized tangential strain rate at $t/\tau_0 \approx 0.8$: a) Case 1; b) Case 2.

Table III. Evolution with time of normalized flamelet speed $\langle s_n \rangle$ (Eq. 18), normalized flame area $\mathcal{L}^*$ (Eq. 18), and normalized turbulent flame speed s_T^* (Eq. 20) for Case 2.

t/τ_0	$\langle s_n \rangle$	$\mathcal{L}^*$	s_T^*
0.0	1.00	1.00	1.00
0.23	0.96	1.10	1.06
0.36	0.91	1.24	1.13
0.80	0.75	1.86	1.40

4.4. Local flame structure

Profiles of heat-release rate and OH mass fraction along the local flame normal are overlaid on the corresponding laminar profiles in Figure 10 for Case 2 at two instants of time. The turbulent profiles have been uniformly sampled along the turbulent flame front; only nine or ten turbulent profiles are shown, for clarity. At the earlier time ($t/\tau_0 = 0.23$), local turbulent profiles collapse neatly onto the steady unstrained laminar contours. At later times ($t/\tau_0 = 0.80$), the collapse remains reasonable on the fresh-gas side while the turbulent profiles generally are shifted inwards towards the peak heat-release zone on the burnt-gas side. This appears to be a consequence of the net extensive tangential strain rates thinning the flame in the turbulent flow and reducing the local flamelet speed while peak heat release rate remains relatively unchanged.

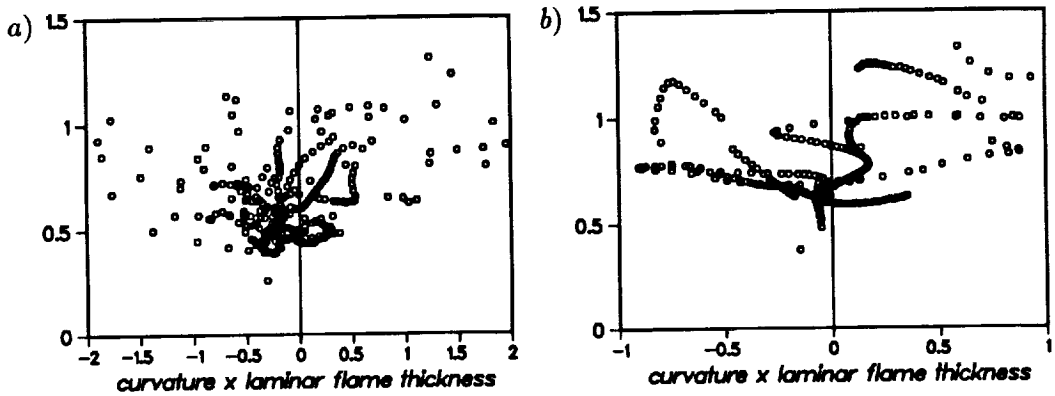

FIGURE 8. Scatter plots of normalized flamelet speed s_n (Eq. 18) versus normalized flame curvature at $t/\tau_0 \approx 0.8$: a) Case 1; b) Case 2.

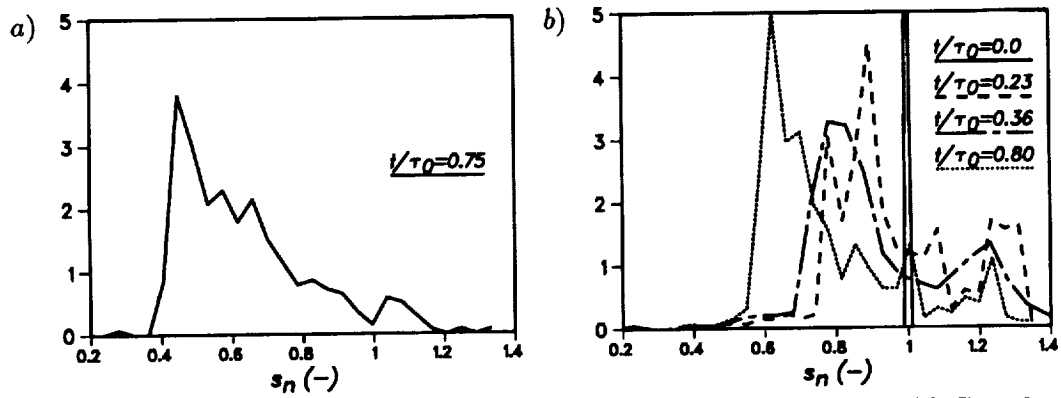

FIGURE 9. Pdf's of normalized flamelet speed s_n (Eq. 18): a) Case 1; b) Case 2.

5. Discussion

Predictive models of turbulent premixed combustion for engineering applications remain at an early stage of development. Key physical processes including ignition and early flame kernel development, complex hydrocarbon–air reaction kinetics, turbulence–chemistry interactions, and flame–wall interaction remain poorly understood even at a fundamental level. Direct numerical simulation has played an increasingly important role in recent years both in contributing to fundamental understanding and in providing guidance for modeling. Fundamental contributions of DNS include elucidation of flame topology and structure (Kerstein *et al.* 1988, Ashurst *et al.* 1988, Rutland & Trouve 1990, Ashurst 1990, Cant *et al.* 1990, Rutland *et al.* 1990, El Tahry *et al.* 1991, Girimaji & Pope 1992), a characterization of the scales of turbulent motion that influence flame structure (Poinsot *et al.* 1990, 1991), flame quenching (Poinsot *et al.* 1991, Meneveau & Poinsot 1990), and thermodiffusive (Lewis number) effects (Rutland & Trouvé 1990, Haworth & Poinsot 1992). Moreover, DNS results have been used to construct and to calibrate models for premixed flame propagation (Bray & Cant 1992), ignition and

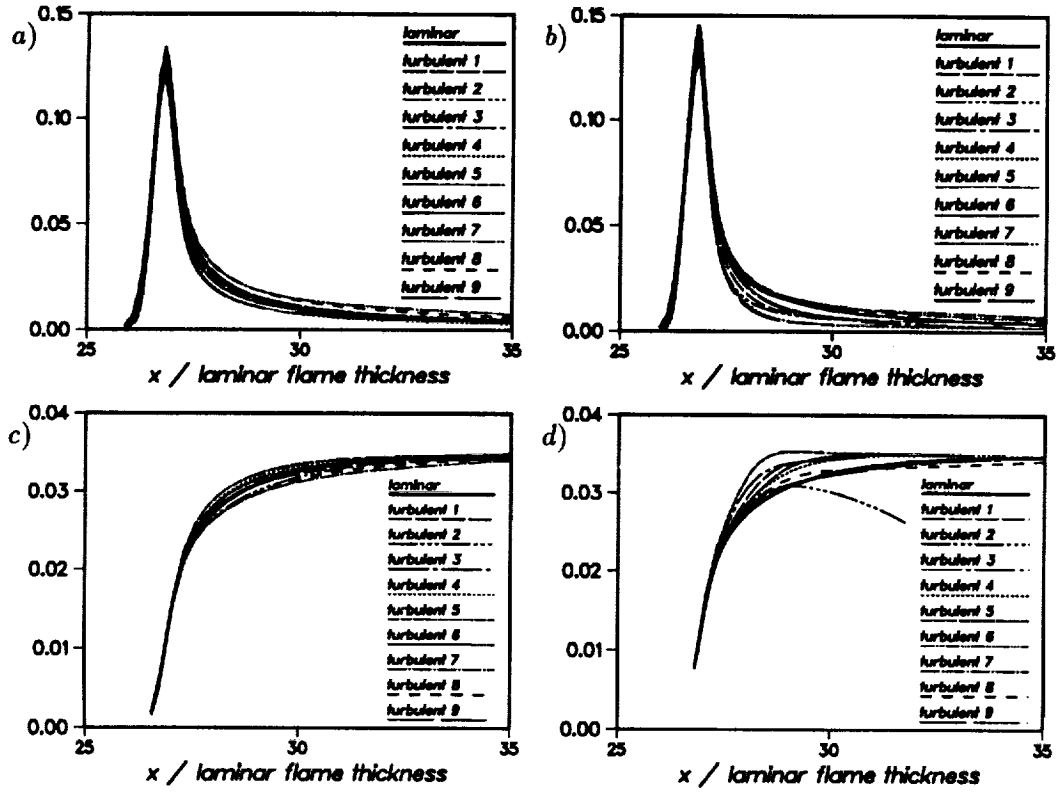

FIGURE 10. Unnormalized laminar and turbulent flame profiles for Case 2: a) heat-release rate, $t/\tau_0 = 0.23$; b) heat-release rate, $t/\tau_0 = 0.80$; c) OH mass fraction, $t/\tau_0 = 0.23$; d) OH mass fraction, $t/\tau_0 = 0.80$.

early flame-kernel growth (Poinsot 1991), and flame-wall interactions (Poinsot & Haworth 1992). These models can be incorporated into multidimensional Reynolds-averaged modeling approaches for engineering devices (e.g. Boudier *et al.* 1992).

The present simulations represent a first attempt to incorporate realistic chemical kinetics and transport into full turbulence simulations. Principle results are: 1) Realistic chemical kinetics and transport have been implemented successfully into full turbulence simulations. 2) Consistent with the simpler models, the complex-chemistry turbulent flame aligns preferentially with extensive strain rates in the tangent plane and flame curvature pdf's are close to symmetric with near-zero means. 3) By contrast to simple chemistry results with non-unity Lewis numbers, local flame structure does not correlate with local flame curvature but rather with local tangential strain rate. Turbulent straining results in substantial thinning of the flame relative to the steady unstrained laminar case. Peak heat-release rate remains close to the laminar value, but integrated heat release along the local flame normal is substantially lower in the turbulent flame. 4) Heat release and H_2O_2 contours remain thin and connected ('flamelet-like') while species including H-atom and OH are more diffuse. In particular, peak OH concentration occurs well behind the peak

heat–release zone.

The strong correlation of s_n with strain rate rather than with curvature (Figures 7 and 8) for the present computations suggests an effective Lewis number that is greater than or equal to unity. However, no amount of straining of the simple–chemistry flames in Haworth & Poinsot (1992) resulted in the extreme thinning and decrease in $\langle s_n \rangle$ than has been observed here. For the present stoichiometric reactants, definition of a single deficient–reactant–based Lewis number is problematic (Joulin & Mitani 1981, Chelliah & Williams 1987). Computations with fuel–lean reactants may help to shed light on these results.

Present turbulence Reynolds numbers and the normalized turbulence intensity u'/s_l^0 (Table II) are typical of values found, for example, in reciprocating internal combustion (IC) engines at low engine speeds. The computed flames remain thick compared to the $l/\delta_l \approx 30$ typical of propane–air mixtures under standard IC–engine operating conditions (stoichiometric, $p = 5$ atm, $T_u = 600$ K, undiluted). However, l/δ_l can be as low as three for high T_u, low p, or high exhaust–gas dilution engine cases (Mantzaras *et al.* 1988; Blint, 1988, 1990). The present choice of initial turbulence spectrum (Haworth & Poinsot 1992) results in too little energy at low wavenumbers compared with classic equilibrium turbulence: thus there is little dissipation in the hot post–flame gas in spite of the high temperature–induced viscosity there. Computations with a more realistic initial spectrum are planned.

The high adiabatic flame temperature (2840 K) for the present thermochemistry results in significant equilibrium levels of fuel and oxidizer in the burnt gas and in high equilibrium radical concentrations of OH, H–atom, and O–atom (Figure 2). Thus it is not surprising that OH serves as a poor marker of the heat–release zone for this flame. The H_2O_2 radical serves better in this regard computationally, but may be a poor choice in practice: peak H_2O_2 mass fraction in the present case is 0.000094 versus 0.0348 for OH. Moreover, the reaction–rate constants involving H_2O_2 in Table I are not well established. Nonstoichiometric and cooler reactants would result in lower temperatures and narrower OH radical profiles. In these cases, OH may better serve as a marker of the reaction zone consistent with the experimental observations of Becker *et al.* (1990), for example.

Further hydrogen–air work thus will include modifications to the initial turbulence spectrum, fuel–lean cases, runs to later times t/τ_f, and additional postprocessing to look at relative shifts in species mass fraction profiles relative to the steady laminar flame. Additional chemistry for NO_x production and extensions to pollutant formation in hydrocarbon–air systems are anticipated subjects for future investigations.

Acknowledgements

The authors acknowledge the fruitful interaction with other members of the combustion group during the 1992 summer program of the CTR. In particular, we thank our CTR host Dr. Arnaud Trouvé.

REFERENCES

ASHURST, W. T. & BARR, P. K. 1983 Stochastic calculation of laminar wrinkled flame propagation via vortex dynamics. *Combust. Sci. & Technol.* **34,** 227–256.

ASHURST, W. T., PETERS, N., & SMOOKE, M. D. 1987 Numerical simulation of turbulent flame structure with non–unity Lewis number. *Combust. Sci. & Technol.* **53,** 339–375.

ASHURST, W. T., SHIVASHINSKY, G. I., & YAKHOT, V. 1988 Flame–front propagation in nonsteady hydrodynamic fields. *Combust. Sci. & Technol.* **62,** 273–284.

ASHURST, W. T. 1990 Geometry of premixed flames in three–dimensional turbulence. In *Proc. 1990 Summer Program,* Center for Turbulence Research, Stanford University & NASA Ames, 245–253.

BATCHELOR, G. K. 1953 *The theory of homogeneous turbulence.* Cambridge University Press.

BECKER, H., MONKHOUSE, P. B., WOLFRUM, J., CANT, R. S., BRAY, K. N. C., MALY, R., PFISTER, W., STAHL, G., & WARNATZ, J. 1990 Investigation of extinction in unsteady flames in turbulent combustion by 2D-LIF of OH radicals and flamelet analysis. *23rd Symp. (Intl.) on Combust.* The Combustion Institute, Pittsburgh, 817–823.

BLINT, R. J. 1988 Flammability limits for exhaust gas diluted flames. *22nd Symp. (Intl.) on Combust.* The Combustion Institute, Pittsburgh, 1547–1554.

BLINT, R. J. 1990 Stretch in premixed laminar flames under IC engine conditions. *Combust. Sci. & Technol.* (to appear).

BOUDIER, P., HENRIOT, S., POINSOT, T., & BARITAUD, T. 1992 A model for turbulent flame ignition and propagation in spark ignition engines. *24th Symp. (Intl.) on Combust.* The Combustion Institute, Pittsburgh, in press.

BRAY, K. N. C. & CANT, R. S. 1991 Some applications of Kolmogorov's turbulence research in the field of combustion. *Proc. R. Soc. Lond. A.* **434,** 217–240.

CANDEL, S. M. & POINSOT, T. J. 1990 Flame stretch and the balance equation for the flame area. *Combust. Sci. & Technol.* **70,** 1–15.

CANT, R. S., RUTLAND, C. J., & TROUVÉ, A. 1990 Statistics for laminar flamelet modeling. In *Proc. 1990 Summer Program,* Center for Turbulence Research, Stanford University & NASA Ames, 271–279.

CHELLIAH, H. K. & WILLIAMS, F. A. 1987 Asymptotic analysis of two–reactant flames with variable properties and Stefan–Maxwell transport. *Combust. Sci. & Technol.* **51,** 129–144.

DRAKE, M. C. & BLINT, R. J. 1988 Structure of laminar opposed–flow diffusion flames with $CO/H_2/N_2$ fuel. *Combust. Sci. & Technol.* **61,** 187–224.

EL TAHRY, S. H. 1990 A turbulence combustion model for premixed charge engines. *Combust. & Flame.* **79,** 122–140.

EL TAHRY, S. H., RUTLAND, S. H., & FERZIGER, J. H. 1991 Structure and propagation speeds of turbulent premixed flames – a numerical study. *Combust. & Flame.* **83,** 155–173.

GHONIEM, A. F. & KRISHNAN, A. 1988 Origin and manifestation of flow/combustion interactions in a premixed shear layer. *22nd Symp. (Intl.) on Combust.* The Combustion Institute, Pittsburgh, 665–675.

GIRIMAJI, S. S. & POPE, S. B. 1992 Propagating surfaces in isotropic turbulence. *J. Fluid Mech.* **234,** 247–277.

HAWORTH, D. C. & POINSOT, T. J. 1992 Numerical simulations of Lewis number effects in turbulent premixed flames. *J. Fluid Mech.* **244,** 405–436.

HERRING, J. R., ORSZAG, S. A., KRAICHNAN, R. H., & FOX, D. G. 1974 Decay of two–dimensional homogeneous turbulence. *J. Fluid Mech.* **66,** 417–444.

JOULIN, G. & MITANI, T. 1981 Linear stability analysis of two–reactant flames. *Combust. & Flame.* **40,** 235–246.

KEE, R. J., MILLER, J. A., & JEFFERSON, T. H. 1980 CHEMKIN: a general–purpose, problem–independent, transportable, FORTRAN chemical–kinetics code package. SANDIA Report No. SAND80–8003.

KEE, R. J., WARNATZ, J., & MILLER, J. A. 1983 A FORTRAN computer code package for the evaluation of gas–phase viscosities, conductivities, and diffusion coefficients. SANDIA Report No. SAND83–8209.

KERSTEIN, A. R., ASHURST, W. T., & WILLIAMS, F. A. 1988 Field equations for interface propagation in an unsteady homogeneous flowfield. *Phys. Rev. A.* **37,** 2728–2731.

LEE, T.–W., NORTH, G. L., & SANTAVICCA, D. A. 1991 Curvature and orientation statistics of turbulent premixed flame fronts. *Combust. Sci. & Technol.* (submitted for publication).

LELE, S. 1992 Compact finite difference schemes with spectral–like resolution. *J. Comp. Phys.* (to appear).

LESIEUR, M. 1987 *Turbulence in Fluids.* Martinus Nijhoff.

MANTZARAS, J., FELTON, P. G., & BRACCO, F. V. 1988 Three–dimensional visualization of premixed–charge engine flames. SAE Paper No. 881635.

MENEVEAU, C. & POINSOT, T. 1990 Stretching and quenching of flamelets in premixed turbulent combustion. *Combust. & Flame.* **86,** 311–332.

MILLER, J. A., MITCHELL, R. E., SMOOKE, M. D. & KEE, R. J. 1982 Toward a comprehensive chemical kinetic mechanism for the oxidation of acetylene: comparison of model predictions with results from flame and shock tube experiments. *19th Symp. (Intl.) on Combust.* The Combustion Institute, Pittsburgh, 181–196.

ORAN, E. S. & BORIS, J. P. 1987 *Numerical simulation of reactive flow.* Elsevier, New York, 416–431.

POINSOT, T., VEYNANTE, D., & CANDEL, S. 1990 Diagrams of premixed turbulent combustion based on direct simulation. *23rd Symp. (Intl.) on Combust.* The Combustion Institute, Pittsburgh, 613–619.

POINSOT, T. 1991 Flame ignition in a premixed turbulent flow. In *Center for Turbulence Research Annual Research Briefs,* Center for Turbulence Research, Stanford University & NASA Ames, 1–22.

POINSOT, T., VEYNANTE, D., & CANDEL, S. 1991 Quenching processes and premixed turbulent combustion diagrams. *J. Fluid Mech.* **228,** 561–606.

POINSOT, T., ECHEKKI, T., & MUNGAL, M. G. 1992 A study of the laminar flame tip and implications for premixed turbulent combustion. *Combust. Sci. & Technol.* **81,** 45–55.

POINSOT, T. & LELE, S. 1992 Boundary conditions for direct simulations of compressible viscous flows. *J. Comp. Phys.* **101,** 104–129.

POINSOT, T. J. & HAWORTH, D. C. 1992 Numerical simulations and modeling of the interaction between turbulent premixed flames and walls. In *Proc. 1992 Summer Program, Center for Turbulence Research,* Stanford University & NASA Ames (in press).

POPE, S. B. 1988 Evolution of surfaces in turbulence. *Intl. J. Engng. Sci.* **26,** 445–469.

POPE, S. B. 1991 Numerical issues in pdf methods. *Fourth International Conference on Numerical Combustion,* St. Petersburg, FL, December 2–4, 1991, 165.

RUTLAND, C. J., FERZIGER, J. H., & EL TAHRY, S. H. 1990 Full numerical simulation and modeling of turbulent premixed flames. *23rd Symp. (Intl.) on Combust.* The Combustion Institute, Pittsburgh, 621–627.

RUTLAND, C. & TROUVÉ, A. 1990 Premixed flame simulations for nonunity Lewis numbers. In *Proc. 1990 Summer Program,* Center for Turbulence Research, Stanford University & NASA Ames, 299–309.

SMOOKE, M. D., LIN, P., LAM, J.K., & LONG, M. B. 1990 Computational and experimental study of a laminar axisymmetric methane–air diffusion flame. *23rd Symp. (Intl.) on Combust.* The Combustion Institute, Pittsburgh, 575–582.

WARNATZ, J. 1981 Concentration–, pressure–, and temperature–dependence of the flame velocity in hydrogen–oxygen–nitrogen mixtures. *Combust. Sci. & Technol.* **26,** 203–213.

WESTBROOK, C. 1991 *Engineering Foundation Meeting on Present and Future Engines for Automobiles*, Santa Barbara, CA, August 25–30, 1991.

XU, Y. & SMOOKE, M. D. 1991 Primitive variable solution of a confined laminar diffusion flame using a detailed reaction mechanism. *Fourth International Conference on Numerical Combustion,* St. Petersburg, FL, December 2–4, 1991, 228–229.